Dielectrophoretic Trapping of Single Bacteria at Carbon Nanofiber Nanoelectrode Arrays†

Prabhu U. Arumugam,*,‡,§ Hua Chen,‡,|| Alan M. Cassell,‡,§ and Jun Li*,‡

NASA Ames Research Center, Moffett Field, California 94035, University Affiliated Research Center of University of California−Santa Cruz, Moffett Field, California 94035, and ELORET, Moffett Field, California 94035

Received: August 7, 2007; In Final Form: October 5, 2007

We present an ac dielectrophoretic (DEP) technique for single-cell trapping using embedded carbon nanofiber (CNF) nanoelectrode arrays (NEAs). NEAs fabricated by inlaying vertically aligned carbon nanofibers in SiO_2 matrix are applied as "points-and-lid" DEP devices in aqueous solution. The miniaturization of the electrode size provides a highly focused electrical field with the gradient enhanced by orders of magnitude. This generates extremely large positive DEP forces near the electrode surface and traps small bioparticles against strong hydrodynamic forces. This technology promises new capabilities to perform novel cell biology experiments at the nanoscale. We anticipate that the bottom-up approach of such nano-DEP devices allows the integration of millions of nanolectrodes deterministically in lab-on-a-chip devices and will be generally useful for manipulating submicron particles.

Introduction

A major focus in biological research is to move from population-based analysis to single-cell analysis in order to understand cellular processes.[1,2] It has broad applications in functional genomics,[3] mRNA analysis,[4] environmental analysis,[5] and bioanalysis.[6] This requires new technologies for massive parallel analysis of individual cells. It is particularly challenging for small cells (such as bacteria) and viruses. Here, we report a new ac dielectrophoretic (DEP) technique for single-cell trapping using embedded carbon nanofiber (CNF) nanoelectrode arrays (NEAs). The nanoelectrode (NE) tip displays an extremely high electric field gradient ($\sim 10^{20}$ V^2 m^{-3}), inducing a DEP force of more than 65 pN under a moderate voltage ($\sim$1.5 V). Single *Escherichia coli* can be captured in a fluid flowing at millimeters per second, significantly more efficient than previous micro-DEP devices. This nano-DEP technique allows the integration of millions of NEs deterministically[7] in lab-on-a-chip devices for parallel, high-throughput analysis.

The first critical step in single-cell analysis is to develop methods that can position cells in a desired location reproducibly. Cell manipulation is achieved by several techniques, including laminar flows in microfluidic devices,[8] as well as optical,[9] magnetic,[10] electro thermal,[11] and electrical[12] methods. Among them, microscale DEP technique[13−16] has been widely used for large cells because the electric field distributions can be precisely controlled by lithographically patterned electrodes in microfluidics down to single-cell resolution, i.e., microns. Capturing smaller particles (bacteria, viruses, prions, etc.) requires further miniaturization of electrode dimensions to hundreds of nanometers. One possible solution is to use one-dimensional nanostructures. It is known that the high aspect ratio nanostructures such as carbon nanotubes (CNTs) improve field emission due to the strong enhancement of electric field strength at the sharp tip.[17] Recently, Torma et al.[18] observed extremely high field gradients ($\sim 10^{23}$ V^2 m^{-3}) with multiwalled CNT DEP for DNA trapping. But the method lacks a precise placement and control of electrode dimensions, much needed for biological studies. Here, we investigated the use of NEAs fabricated by inlaying vertically aligned CNFs (50−200 nm diameter) in SiO_2 matrix as a DEP trap in aqueous solution.

DEP is based on the polarization of particles in a nonuniform electric field.[19] The time-average DEP force on the particle in a sinusoidal field is $\langle \mathbf{F}_{dep}(\mathbf{r}) \rangle = \pi \epsilon_m R^3 Re[K(\omega)] \cdot \nabla |\mathbf{E}(\mathbf{r})|^2$ where ϵ_m is the permittivity of the medium, R is the particle radius, $Re[K(\omega)]$ is the real part of the complex Clausius−Mossotti factor $K = (\epsilon_p - \epsilon_m)/(\epsilon_p + 2\epsilon_m)$, defined by the angular frequency (ω) dependent complex permittivity of the medium (ϵ_m) and particle (ϵ_p). For $\epsilon_p > \epsilon_m$, as in the case of cells and viruses, $Re[K(\omega)]$ is positive and particles move toward higher electric field, resulting in positive DEP (pDEP). The magnitude is proportional to $\nabla |\mathbf{E}(\mathbf{r})|^2$, determined by the electrode geometry and voltage. For a NE, $\nabla |\mathbf{E}(\mathbf{r})|^2$ can be increased by orders of magnitude, generating a much stronger DEP force. We demonstrate that the large pDEP force is able to counter Stokes drag force in a high-velocity laminar microfluidic flow and effectively traps *E. coli* at individual NEs.

In Figure 1a, a "points-and-lid" geometry is employed where an embedded NEA is placed at the bottom of a microchannel with a large indium−tin oxide (ITO) coated glass counter electrode at the top. This geometry generates a highly asymmetric electric field focusing at the separated NE points, ideal for pDEP trapping of single cells.[14,15] In this study, a vertically aligned CNF is encapsulated by SiO_2, leaving only the tip exposed at the planarized surface (Figure 1b), resulting in an array of point NEs.

Experimental Section

Device Fabrication. Our approach consists of six major steps extended from the previously reported method in fabrication of inlaid CNF NEAs:[7] (1) metal deposition for electrical contacts

† Part of the "Giacinto Scoles Festschrift".

* Corresponding authors. (J.L.) Phone: 408 718 7142. E-mail: junli@ksu,edu. Current address: Kansas State University, Department of Chemistry, Manhattan, KS 66506. (P.U.A.) Phone: 650 604 4338. E-mail: paramugan@arc.nasa.gov.

‡ NASA Ames Research Center.

§ University of California−Santa Cruz.

|| ELORET.

10.1021/jp076346e CCC: $37.00 © 2007 American Chemical Society
Published on Web 11/14/2007

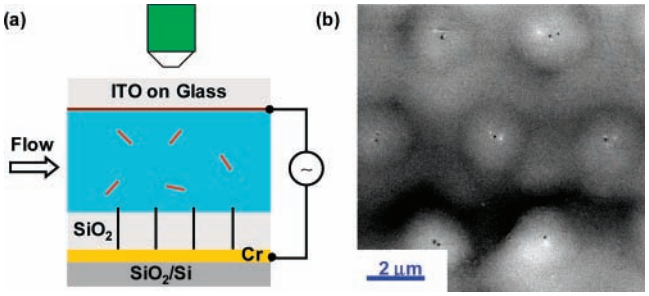

Figure 1. Carbon nanofiber nanoelectrode array based DEP chip. (a) Layout showing the points-and-lid electrode arrangement of carbon nanofiber (CNF) DEP electrodes at the bottom and indium tin oxide counter electrode at the top of the microchannel. The electrodes are separated by a patterned SU-8 polymer, which also forms the seal for the microchannel. (b) SEM image of the top view of an inlaid regular CNF nanoelectrode array that was patterned by e-beam lithography.

and as catalyst for CNF growth, (2) directional growth of CNF by plasma-enhanced chemical vapor deposition (PECVD), (3) SiO_2 encapsulation of CNF by tetraethylorthosilicate (TEOS) CVD for electrical isolation and mechanical stability, (4) reactive ion etching (RIE) and chemical mechanical polishing (CMP) to expose CNF tips on the planarized SiO_2 matrix, (5) SU-8 patterning to form the microchannel and to bond the ITO/glass substrate that serves as counter electrode and channel cover, and (6) fluidic and electrical packaging. The process sequence for this fabrication process is shown in Figure 2. The details of each process step are as follows:

(1) Electron beam deposition (Innotech ES26C) was used for the deposition of chromium (~200 nm) followed by an active catalyst (nickel, ~30 nm) on a 4 in. silicon (100) wafer covered with 500 nm of thermal oxide (Silicon Quest International, Inc, Santa Clara, CA).

(2) A forestlike vertically aligned CNF was grown on nickel catalyst by PECVD using a dc-bias in a custom-made chamber. The operating parameters for growth were 80 sccm ammonia, 22.5 sccm acetylene, 4−4.5 Torr, and 510 W. A 10 min deposition yields 50−200 nm diameter and ~5 μm long fibers. Each CNF was vertically aligned and freestanding on the surface (Figure 2b).

(3) A SiO_2 film was deposited by thermal CVD using TEOS at a vapor pressure of ~400 mTorr and at a temperature of 715 °C in a quartz-tube furnace. SiO_2 formed a conformal film, filling the free space between the individual fibers as well as the substrate (Figure 2c). An 8 h deposition ensured complete coverage of the CNFs.

(4) The excess SiO_2 and part of the CNFs were removed by the combination of CMP and RIE. The initial planarization of the dielectric surface was done manually using 0.3 μm Alpha micropolish alumina (Buehler, Lake Bluff, IL). Dry plasma etching (Phantom II RIE system, Trion Tech, Clearwater, FL) was then used to etch down SiO_2 and expose CNF tips. Oxygen (7 sccm) and CHF_3 (5 sccm) gases at 100 W and 150 mTorr were used to etch the dielectric. The number of CNF tips exposed (array density) was easily controlled by the etching time. Measuring the electrical resistance between two points at the surface was used to monitor the progress of the etching and the number of fibers exposed. A CMP step might be followed to clean up the debris and ensure a planized surface. In this study, we used low-density samples with an average fiber−fiber spacing over 10 μm to avoid any overlap of the electric fields from the neighboring nanoelectrodes so that each one behaves as a single trap site. The large spacing also made it easier for us to observe individual bacteria at each site. For a better illustration of the exposed tips, we show a high-density array (average fiber−fiber spacing of ~500 nm) in Figure 2d. Scanning electron microscope images were taken using an Hitachi S-4000 microscope.

(5) For microchannel fabrication and ITO-glass bonding, the silicon substrate was rinsed several times in acetone, blow-dried in air, and dehydrated in a Blue M oven at 150 °C for 30 min. Then SU-8 2010 (Microchem, Newton, MA) was spin coated (3000 rpm, 30 s; Headway, Garland, TX), soft baked (65 °C for 60 s and 95 °C for 90 s, on a hot plate), UV exposed (15 s, soft contact mode; Karl Suss MA-6, Germany) using Mylar masks (Advanced Reproductions Corp., North Andover, MA), postbaked (65 °C for 60 s and 95 °C for 90 s, on a hot plate), developed (SU-8 developer; Microchem, Newton, MA), and spray-dried in IPA and air. The thickness of the SU-8 layer was ~10 μm. Then the above process was repeated on the ITO−glass substrate with few exceptions. The soft bake was done at 65 °C for 90 s followed by placing it on the silicon-SU-8 substrate kept on a 75 °C hot plate. The glass substrate was gently pressed starting from the center with a pair of tweezers. The assembly was held at 75 °C for 5 min and slowly cooled to room temperature by switching off the hot plate. Procedures including UV exposure, postbake, drilling reservoir holes (1.1 mm diamond bits; Abrasive Technology), developing, and sonicating in SU-8 developer were followed before the chip was ready for fluidic and electrical packaging (Figure 2e).

(6) Thirty gauge wire wraps (Page Digital Inc.) were epoxied to the electrical pads on CNF NEA and ITO (silver conductive epoxy; MG Chemical). Aluminum bushing (custom-made) was then bonded to the reservoirs using port adhesives (N-100-01; Upchurch Scientific, Oak Harbor, WA). The fluidic inputs from the syringe and peristaltic pumps (Model 3200; FIALab Instruments Inc., Bellevue, WA) were press-fitted to the bushing.

***E. coli* Culture and Labeling.** Frozen *E. coli* stock (DHα5) was supplied by Invitrogen (Carlsbad, CA). The bacterial stock was thawed on ice for 30 min and inoculated into 1 mL of LB medium in a 1.5 mL Eppendorf tube. The bacteria were grown for 2 h at 37 °C in an incubator. A small portion of them was transferred to an agar plate and incubated overnight. A single bacterial colony was picked from the plate and grown in 3 mL of LB nutrient broth and into the late log phase to a cell concentration of $\sim 1 \times 10^9$ cells/mL (overnight). The cells were centrifuged at 5000 rpm for 10 min to eliminate the LB nutrient broth and a concentration of $\sim 1 \times 10^9$ live cells was resuspended in 1 mL of PBS using a vortex mixer. For labeling, the cells were incubated with goat anti-*E. coli* Ab at 2 μg/mL for 2 h on ice (Biodesign, Saco, ME), pelleted, and washed with PBS three times and then resuspended in 1 mL of PBS. Finally, the cells were incubated in Alexa 594 conjugated chicken anti-goat second Ab at 2 μg/mL for 2 h on ice, pelleted, washed with PBS three times, and resuspend in DI water at the desired concentration for DEP experiments.

DEP Experiments. The DEP chip was placed under the objective (20×) of an upright optical microscope (470−550 nm filter, Axioskop 2 FS; Carl Zeiss) in reflection mode with the field view halfway between the microchannel reservoirs. An AxioCamMR digital camera was used to take fluorescence images. The images were captured at 1 fs and 0.4 s exposure. Sine wave excitation at 0.5, 1, and 10 MHz was generated by an Agilent 33220A signal generator (Agilent, Palo Alto, CA). The microchannel was thoroughly rinsed with DI water to remove any nonspecifically bound *E. coli* using the peristaltic pump (~150 μL/min, 1 min). Note: Some experiments show

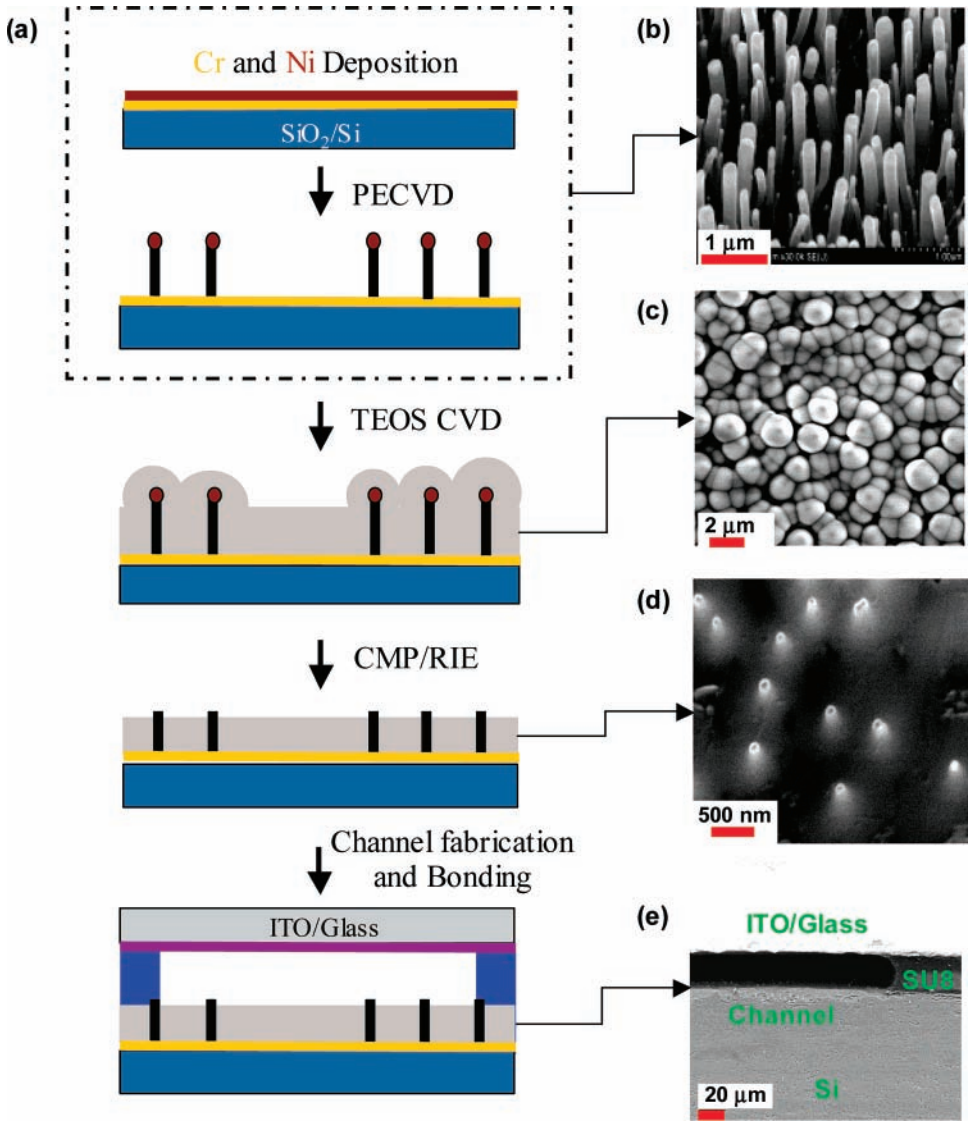

Figure 2. Protocol of DEP device fabrication. (a) Schematics of the process sequence. (b) SEM image of vertically aligned as-grown CNFs (45° view). (c) SEM image of CNFs after being encapsulated with SiO_2 (top-down view) (d) SEM image of the top surface of an embedded CNF after reactive ion etching and chemical mechanical polishing (45° view). (e) Cross sectional view of the final DEP device.

that we have nonspecific binding, but it is negligible based on the fluorescent signal. The *E. coli* suspension was then injected into the channel at the desired flow rate using the syringe pump. Once the flow is stabilized, the camera was turned on to capture the images. After a certain time (~10 s), the electrodes were energized to the desired voltage for a specific time (~30 s) to trap *E. coli*. Then the voltage was turned off to observe the release from NEs (~10 s). The trap strength was determined by a (rate of) change in the fluorescence intensity. A higher intensity suggests stronger traps. The minimum voltage was determined to be the voltage at which the NEs starts trapping, as observed through the microscope. Then the procedure was repeated for two different flow velocities (250 μm/s, 0.15 μL/min; 2 mm/s, 1.2 μL/min) and voltages ($V_{pp} = 0-9$ V).

DEP Modeling. Modeling was performed using a multiphysics finite element modeling software (CFD-ACE$^+$, ESI Group Inc.). The steps needed to simulate DEP trapping of particles in a micro flow include geometry generation, grid generation, problem setup, solution generation, and postprocessing, all done using CFD-ACE$^+$. The 2D model, in this case a microfluidic channel 20 μm high and 102 μm long with a linear array of 12 NEs placed at the bottom, takes the electric, flow, and spray parameters to compute the particle trajectory, consisting of the DEP force, hydrodynamic force, and gravity. The NEs were 200 nm wide and separated by 2 μm. The 2-μm separation was chosen to eliminate the field overlapping from nearby electrodes. By varying the flow velocity, voltage, or both for a given experimental run, the modeling software can determine the maximum particle heights below which all particles are trapped. The geometry simulated is representative of the experimental parameters, even though the model length is only 102 μm (the experimental channel length is ~12 000 μm) because the interest is only near the electrode array where significant changes in the field gradients are expected. Therefore, the results are not compromised. The boundary conditions were electric potential on the electrodes, electric insulation on the outer surfaces, ac frequency, and flow velocity at the inlet. The simulations were performed on 1 μm diameter spherical particles with a particle density of 1100 kg/m^3, medium density of 1000 kg/m^3, particle conductivity of 3×10^{-2} S/m, and relative permittivity of 400, in media with a conductivity of 2×10^{-4} S/m and a relative permittivity of 80. The particle properties were chosen on the basis of data for *E. coli* found in the literature.[20,21] The applied signal was a sine wave of 1 MHz.

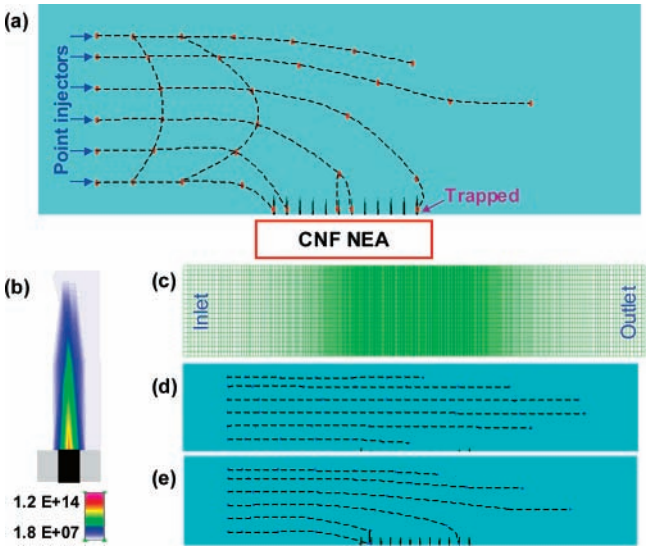

Figure 3. Modeling of pDEP trapping on CNF NE array. (a) Trapping of 1 μm diameter particles under the influence of Stokes drag and dielectrophoretic forces at 26 V V_{pp}. The flow velocity is 10 mm/s. The dashed lines show the particle trajectory. (b) Mapping of the square of electric field strength around the NE surface with a linear color scale. (c) Structured grid of the channel geometry. (d and e) Particle trajectories at $V_{pp} = 2$ and 9 V, respectively at a flow velocity of 2 mm/s. Note: The particles are introduced from point injectors at different heights from the electrode surface (3, 6, 9, 12, 15, and 17 μm).

Results and Discussion

The most important consideration in cell trapping is to know the strength of the DEP forces. Strong DEP forces can counteract the drag force better and thus facilitate quick cell loading. Ideal DEP traps need to be operated at low voltages to avoid any cell damage and at high flow rates to process large sample volume quickly. We performed two-dimensional (2D) finite element modeling of pDEP trapping at a linear array of 12 CNF NEs as a function of voltage and flow velocity. As shown in Figure 3a, particles of 1 μm in diameter are injected at various heights, simulating *E. coli*. The trajectories show that all particles injected below 12 μm height are trapped, while others (including those near the ceiling) are deflected downward. A larger array may trap all particles. The flow velocity (10 mm/s) is much higher than those in a micro-points-and-lid device (0.1−0.5 mm/s)[15] or interdigitated device (0.04−2 mm/s),[16] reflecting the higher trapping efficiency. The $\mathbf{E}(\mathbf{r})^2$ map around a NE tip (Figure 3b) shows a maximum of $\sim 1.2 \times 10^{14}$ V^2 m^{-2}, 200 times higher than that of the micro-points-and-lid device.[15] Figure 3c shows the structured grid of the microchannel geometry that was divided into 7790 cells with the smallest grid size being 100 nm located at the NE tip. Figure 3, parts d and e, shows the particle trajectory at lower voltages ($V_{pp} = 2$ and 9 V) at 2 mm/s flow velocity. At $V_{pp} = 2$ V, only particles injected at the height ≤ 3 μm are trapped and all others above are not influenced by the DEP. At $V_{pp} = 9$ V, particles injected at ≤ 9 μm are trapped and even those above are deflected downward.

Figure 4 shows the field gradients and the magnitudes of the drag and dielectrophoretic forces at different heights away from the tip of a nanoelectrode. These data are derived from the 2D simulation shown in Figure 3 with the lateral *x*-axis along the microfluidic channel and the vertical *y*-axis normal to the NEA surface. Clearly, the vertical field gradient (∇E_y^2) is proportional to V_{pp}^2 and drops rapidly within ~ 5 μm from the NE surface. It then decreases much slower beyond this range. The vertical component dominates the field gradient for the height over 5 μm, while the lateral component (∇E_x^2) dominates below ~ 3 μm height as indicated by the overlapping of ∇E^2 and ∇E_y^2 points over 3 mm height in Figure 4b. These analyses indicate that particles are first pulled down toward the NEs by the vertical pDEP force orthogonal with the drag force. Once within ~ 3 μm from the NE surface, the particles encounter a lateral pDEP force orders of magnitude higher than the drag force (as shown in Figure 4c) so that they are firmly trapped at the nearest NE sites.

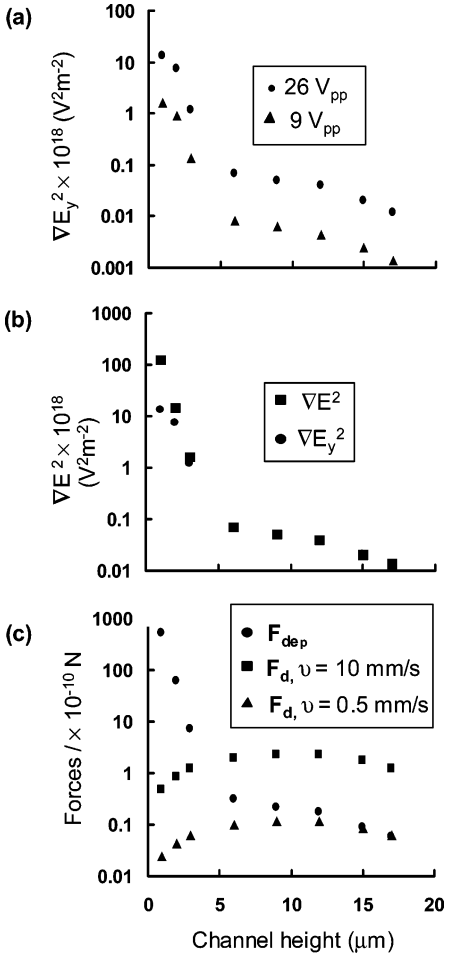

Figure 4. Comparison of electric field strength gradients and magnitudes of drag and dielectrophoretic forces. (a) Gradient of vertical electric field strength (∇E_y^2) at $V_{pp} = 26$ and 9 V (log scale). (b) Gradient of vertical (∇E_y^2) and total ($\nabla \mathbf{E}^2$) field strength at $V_{pp} = 26$ V (log scale) where $\nabla E^2 = \nabla E_x^2 + \nabla E_y^2$. (c) Magnitude of forces at $V_{pp} = 26$ V (log scale). The drag force on a spherical particle is given by $6\eta\pi R k \upsilon$, where η is the dynamic viscosity, k is a factor that accounts for wall effects (1.7 for a particle in contact with the wall), R is the particle radius, and υ is the flow velocity.

To prove this, we fabricated the NEA DEP device in a straight microchannel of 500 μm (W) × 20 μm (H) × 2 cm (L) (as illustrated in Figure 2e). An ac potential is applied between the NEA and the ITO electrode. The ac field allows cell manipulation with minimum electro-osmosis, electrochemical reaction, joule heating, and cell membrane disruption. We first evaluate the trap performance by measuring the integrated fluorescence intensity from stained *E. coli* by focusing in a ~ 0.25-mm^2 area at the bottom of the channel. An *E. coli* suspension ($\sim 1 \times 10^9$/mL) is continuously passed through the microchannel. The trap is turned on and off to observe how *E. coli* are captured and released from the NEA. The DEP voltage is varied between $V_{pp} = 0$ and 9 V in a series of experiments. As shown in Figure 5a, at a flow velocity of ~ 2 mm/s, we need only $V_{pp} = 1$ V to initiate trapping. At $V_{pp} \leq 3$ V, the fluorescence intensity

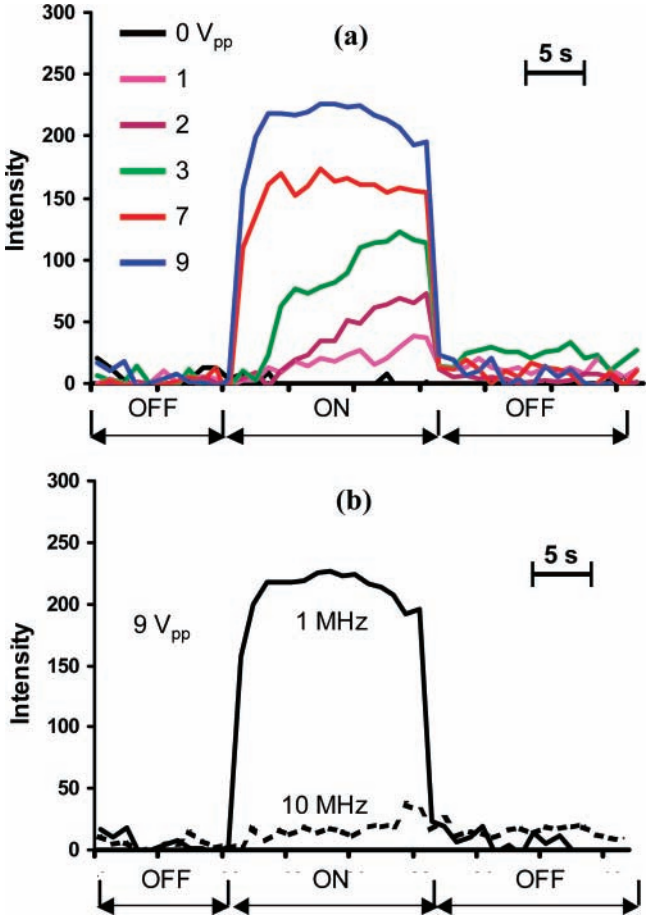

Figure 5. (a) Epifluorescence change as a function of voltage. (b) The comparison of the DEP trapping at 1 and 10 MHz, respectively. The flow velocity in both experiments is ~2 mm/s.

increases slowly, with the slope rate proportional to V_{pp}^2. At $V_{pp} > 3$ V, it quickly saturates within 3 s. This shows that CNF NEs are able to generate stronger DEP force to trap *E. coli* with applied V_{pp} similar to other state-of-the-art DEP devices. Thus, much lower voltages can be used to generate forces with magnitudes similar to others. This significantly mitigates cell damage and minimizes undesirable convectional flows caused by joule heating, which is critical for in vitro cell biology studies. The frequency dependence studies show similar performance at 1 and 0.5 MHz, respectively. But the bacteria trapping at 10 MHz is negligible (see Figure 5b), confirming previous observations of the decrease in polarizability of bacteria at higher frequencies.[22] The positive DEP observed at ≤1 MHz is specific to the DHα5 *E. coli* strain used in this study. This will vary with the type of bioparticle.

The simulation and experimental results are in good agreement even though only a 2D linear NEA and simple bioparticle model are employed. As shown by the simulation in Figure 3d, only particles close to the electrode surface (≤3 μm) are trapped at low voltages ($V_{pp} < 2$ V). Either a larger linear array or a higher voltage is required to increase the trapping efficiency. At $V_{pp} = 9$ V, Figure 3e shows that even particles injected at ~9 μm are trapped and others above are significantly deflected. It is possible to capture all particles instantaneously in a rather short array (~50 μm) at $V_{pp} = 9$ V, which is consistent with the experimental results in Figure 5. The saturation of fluorescence intensity indicates that all available NE sites are occupied by *E. coli* quickly after the electrode is energized.

The trapping and release of *E. coli* at individual NE sites is illustrated in Figure 6 by a series of images taken from a DEP

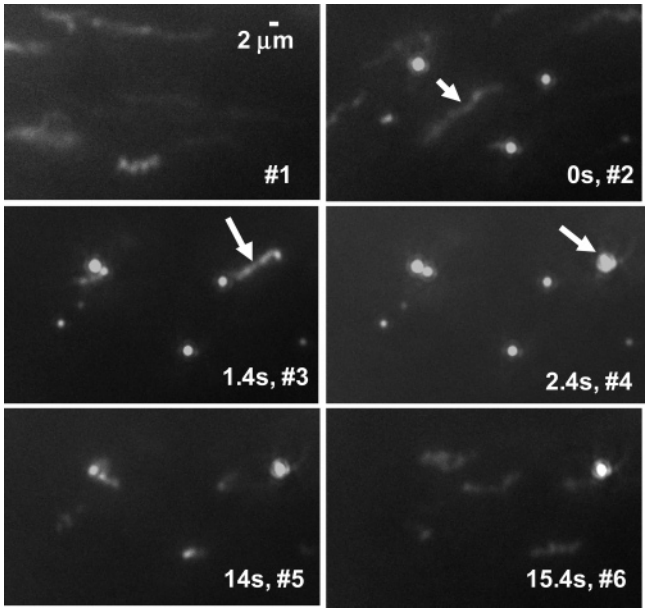

Figure 6. Epifluorescence images showing *E. coli* trapping and release at CNF NEs. The applied voltage is 3 V at 1 MHz and the velocity is ~250 μm/s. The arrows point toward the trajectory of a single *E. coli* while the solution flows from left to right.

movie (see the movie in the Supporting Information). When V_{pp} is off at the beginning (frame 1), *E. coli* bacteria are floating in water and generate fuzzy stretched tracks. After a 3 V V_{pp} is turned on ($t = 0$ s, frame 2), four bacteria are instantaneously snapped onto the exposed CNF tips, generating sharp bright spots, while others are still floating. The arrows highlight the trajectory of one *E. coli*. At $t = 0$ and 1.4 s (frames 2, 3), it passes by a CNF that has already trapped a bacterium. But it is quickly trapped at the next available CNF site at $t = 2.8$ s (frame 4). The *E. coli* with the size of ~1 μm in diameter and ~2 μm in length, which is much larger than the size of the exposed CNF tip of ~100 nm in diameter, can strongly block the local electric field of a CNF NE site. Hence, most CNF sites trap only one bacterium. Only in a few cases multiple bacteria have been observed close to a single NE site. The snapshot at $t =$ 2.4 s, for example, shows two bacteria trapped next to each other at a single NE site. When the V_{pp} is turned off (frames 5, 6), all bacteria are quickly released and washed downstream by the flow. On the basis of the fluorescence intensity shown in Figure 5, we estimate that 100% of bacteria are released when 9 V V_{pp} is turned off in a 2 mm/s flow stream. From the fluorescence images (as shown in the video in Supporting Information), we estimate that 85% of the bacteria are released after the voltage (3 V V_{PP}) is turned off in a 250 micron/s flow stream. By choosing an appropriate voltage and flow velocity, the nano-DEP device can be used as a reversible active filter, even though the cells are subject to a higher gradient field than the traditional interdigitated electrodes.

Conclusions

In summary, we have demonstrated the use of embedded CNF NEA in trapping small bioparticles against strong hydrodynamic drag forces in a microfluidic channel. Two possible scenarios for further application of this new nano-DEP technique can be envisioned, including (1) a low-density array for registration and the study of single particles and (2) a high-density array that is tailored as an active DEP filter for sorting, separating, and concentrating bioparticles. The dimension and the density of the NEA may need to be optimized for different applications

in connection with the microfluidic design. By minor modification, this method can be extended for cell lysing, electroporation, and ultrasensitive biosensing.[23] Our future studies will be concentrated on the development of array-within-an-array DEP trapping sites for multiplex, antibody-based cell manipulation and detection. Our approach of manipulating submicron bioparticles with highly focused, strong electrical fields at NEAs promises new capabilities for cell biology research and the development of highly integrated biochips for environmental and security monitoring.

Acknowledgment. Work was performed in part at the Stanford Nanofabrication Facility of NNIN supported by the National Science Foundation under Grant ECS-9731293. We thank Kartik Shah of ESI Group, for helpful discussions in DEP modeling.

Supporting Information Available: A movie showing the real-time trapping of *E. coli* at NEA sites in a microfluidic flow while the V_{pp} is switched on and off. This material is available free of charge via the Internet at http://pubs.acs.org.

References and Notes

(1) Liu, W. F.; Chen, C. S. *Mater. Today* **2005**, *8*, 28.
(2) Brehm-Stecher, B. F.; Johnson, E. A. *Microbiol. Mol. Biol. Rev.* **2004**, *63*, 538.
(3) Lidstrom, M. E.; Meldrum, D. R. *Nature* **2003**, *1*, 158.
(4) Eberwine, J. *Nat. Neurosci*. **2001**, *4*, 1155.
(5) Le, X. C.; Zhao, Q. *Anal. Bioanal. Chem.* **2007**, *387*, 45.
(6) Hornblower, B.; Coombs, A.; Whitaker, R. D.; Kolomeisky, A.; Picone, S. J.; Meller, A.; Akeson, M. *Nat. Methods* **2007**, *4*, 315.
(7) Li, J.; Ng, H. T.; Cassell, A.; Fan, W.; Chen, H.; Ye, Q.; Koehne, J.; Han, J.; Meyyappan, M. *Nano Lett.* **2003**, *3*, 597.
(8) Takayama, S.; McDonald, J. C.; Ostuni, E.; Liang, M. N.; Kenis, P. J.; Ismagilov, R. F.; Whitesides, G. M. *Proc. Natl. Acad. Sci. U.S.A.* **1999**, *96*, 5545.
(9) Ashkin, A.; Dziedzic, J. M.; Yamane, T. *Nature*. **1987**, *330*, 769.
(10) Koschwanez, J. H.; Carlson, R. H.; Meldrum, D. R. *Rev. Sci. Instrum.* **2007**, *78*, 044301.
(11) Chronis, N.; Lee, L. P. *J. Microelectromech. Syst.* **2005**, *14*, 857.
(12) Rosenthal, A.; Voldman, J. Dielectrophoretic traps for single-particle patterning. *Biophys. J*. **2005**, *88*, 2193.
(13) Voldman, J. *Annu. Rev. Biomed. Eng.* **2006**, *8*, 425.
(14) Albrecht, D. R.; Tsang, V. L.; Sah, R. L.; Bhatia, S. N. *Lab Chip* **2005**, *5*, 111.
(15) Gray, D. S.; Tan, J. L.; Voldman, J.; Chen, C. S. *Biosens. Bioelectron*. **2004**, *19*, 1765.
(16) Li, H.; Zheng, Y.; Akin, D.; Bashir, R. *J. Microelectromech. Syst.* **2005**, *14*, 103.
(17) Nilsson, L.; Groening, O.; Emmenegger, C.; Kuttel, O.; Schaller, E.; Schlapbach, L.; Kind, H.; Bonard, J-M.; Kern, K. *Appl. Phys. Lett.* **2000**, *76*, 2071.
(18) Tuukkanen, S.; Toppari, J. J.; Kuzyk, A.; Hirviniemi, L.; Hytonen, V. P.; Ihalainen, T.; Torma, P. *Nano Lett.* **2006**, *6*, 1339.
(19) Pohl, H. A. *Dielectrophoresis: The Behavior of Neutral Matter in Nonuniform Electric Fields*; Cambridge University Press: New York, 1978.
(20) Martinez-Salas, E.; Martin, J. A.; Vicente, M. *J. Bacteriol.* **1981**, *147*, 97.
(21) Carstensen, E. L.; Cox, H. A.; Mercer, W. B.; Natale, L. A. *Biophys. J.* **1965**, *5*, 289.
(22) Asami, K.; Hanai, T.; Koizumi, N. *Biophys. J.* **1980**, *31*, 215.
(23) Koehne, J. E.; Chen, H.; Cassell, A. M.; Ye, Q.; Han, J.; Meyyappan, M.; Li, J. *Clin. Chem.* **2004**, *50*, 1886.